Density-functional theory for polymer-carbon dioxide mixtures: A perturbed-chain SAFT approach

Xiaofei Xu, Diego E. Cristancho, Stéphane Costeux, and Zhen-Gang Wang

Citation: J. Chem. Phys. **137**, 054902 (2012); doi: 10.1063/1.4742346
View online: http://dx.doi.org/10.1063/1.4742346
View Table of Contents: http://jcp.aip.org/resource/1/JCPSA6/v137/i5
Published by the American Institute of Physics.

Density-functional theory for polymer-carbon dioxide mixtures: A perturbed-chain SAFT approach

Xiaofei Xu,[1] Diego E. Cristancho,[2] Stéphane Costeux,[2] and Zhen-Gang Wang[1,a)]
[1]*Division of Chemistry and Chemical Engineering, California Institute of Technology, Pasadena, California 91125, USA*
[2]*The Dow Chemical Company, Midland, Michigan 48674, USA*

(Received 12 June 2012; accepted 20 July 2012; published online 7 August 2012)

We propose a density-functional theory (DFT) describing inhomogeneous polymer-carbon dioxide mixtures based on a perturbed-chain statistical associating fluid theory equation of state (PC-SAFT EOS). The weight density functions from fundamental measure theory are used to extend the bulk excess Helmholtz free energy to the inhomogeneous case. The additional long-range dispersion contributions are included using a mean-field approach. We apply our DFT to the interfacial properties of polystyrene-CO_2 and poly(methyl methacrylate) CO_2 systems. Calculated values for both solubility and interfacial tension are in good agreement with experimental data. In comparison with our earlier DFT based on the Peng-Robinson-SAFT EOS, the current DFT produces quantitatively superior agreement with experimental data and is free of the unphysical behavior at high pressures (>35 MPa) in the earlier theory. © *2012 American Institute of Physics*. [http://dx.doi.org/10.1063/1.4742346]

I. INTRODUCTION

In a recent paper,[1] we proposed a density functional theory (DFT) for polymer-carbon dioxide (CO_2) mixtures by constructing the free energy functional from a Peng-Robinson statistical associating fluid theory equation of state (PR-SAFT EOS).[2] The theory satisfactorily captures the phase behavior of the mixtures and reproduces the experimental results of interfacial tension at low to moderate pressure. At high pressures ($P > 35$ MPa), however, the PR-SAFT EOS produces some unphysical features with regard to the relative locations of the coexistence curves and the spinodal. In the density-density phase diagram, the binodal curves terminate at an end point at high pressure. Above that pressure, the spinodal curves extend beyond the region enclosed by binodal curves. Predictions from the PR-SAFT-based DFT, especially those concerning the metastability and interfacial properties, become unreliable at $P > 35$ MPa due to this unphysical behavior. Since some industrial processes like polymer foaming by CO_2 in the fabrication of novel porous materials typically operate with initial pressures around 35 MPa or more, it is necessary to develop a more accurate DFT that remains valid at these very high pressures.

The unphysical behavior of PR EOS originates from the poor description of excluded volume effect.[3,4] Perturbed-chain (PC) SAFT EOS (Ref. 5) models the hard-sphere fluids by the Carnahan-Starling equation[6] that gives a better description for the excluded volume effect than the PR EOS does. We thus expect that the artificial behavior at high pressures will be absent in the PC-SAFT EOS. The PC-SAFT EOS is widely used in engineering and can be successfully applied to a variety of substances ranging from small molecules to organic solvents, and particularly to polymers with high molecular weights.[7] It describes the correlations due to chain connectivity and associating interactions by SAFT. As the main advantage, PC-SAFT EOS accounts for the chain-length dependence in the dispersion interactions by perturbation from a chain-like reference fluid, rather than from a monomeric reference fluid. The dispersion interactions between two chains are described by an average chain segment-segment radial distribution function. The volume integrals with respect to chain dispersion interaction are then simplified by a polynomial of the density up to order six. The coefficients of the polynomial are obtained by fitting the calculated binodal with experimental data for a great number of species.[5] This numerical simplification greatly facilitates the mathematical calculations. These virtues make PC-SAFT EOS a widely used EOS for polymers in engineering.[7,8]

Gross[9] proposed a PC-SAFT EOS-based DFT, where the free energy functional for the dispersion interaction is approximated as a first-order perturbation. The functional is not consistent with the dispersion part of the free energy in the bulk EOS and the difference is locally absorbed by an *ad hoc* shift in the chemical potential. Such an approach can only work when the difference in the free energy between the functional and EOS is small enough in the entire range of the thermodynamic states, a requirement that is too strong to be met by all, or even most substances. In this work, by using the weight density functions of Rosenfeld,[10] we construct a functional that is fully consistent with the bulk free energy of the PC-SAFT EOS. The additional long-range dispersion contributions due to spatial inhomogeneity are included using a mean-field approach. We then apply our DFT to examine the phase behavior and interfacial properties of polystyrene (PS)-CO_2 and poly(methyl methacrylate) (PMMA)-CO_2 mixtures.

a)Electronic mail: zgw@caltech.edu.

II. THEORY

A. Molecular model

We consider a compressible polymer-CO_2 mixture, where the molecular units of both components are coarse-grained as spherical particles with a hard core. The CO_2 molecule is modeled as a particle of diameter σ_1. The association interaction between the attractive sites of carbon and oxygen atoms leads to the formation of dimers, trimers, tetramers, etc. We account for the strength of the association interaction by the average size of the clusters, which is denoted as N_1. Best numerical fitting (described in Sec. II B) yields $N_1 = 2$; this value will be used throughout our calculations. A polymer is modeled as a freely joint chain with N_2 identical segments of diameter σ_2 tangentially connected. Mathematically, chain connectivity is enforced by the bonding potential between nearest-neighbor segments,

$$\exp\left[-\beta V_B(\boldsymbol{r}^{N_2})\right] = \prod_{i=1}^{N_2-1} \frac{\delta(|\boldsymbol{r}_{i+1} - \boldsymbol{r}_i| - \sigma_2)}{4\pi\sigma_2^2}, \quad (1)$$

where δ is the Dirac delta function and $\boldsymbol{r}^{N_2} = (\boldsymbol{r}_1, \boldsymbol{r}_2, \ldots, \boldsymbol{r}_{N_2})$ and $\beta^{-1} = kT$ stands for the temperature multiplied by the Boltzmann constant. The interaction between two arbitrary species (i.e. polymer segments or CO_2) is described by

$$u_{ij}^{LJ}(r) = \begin{cases} \infty & r < \sigma_{ij} \\ -\epsilon_{ij}^{LJ}(\sigma_{ij}/r)^6 & r \geq \sigma_{ij} \end{cases}. \quad (2)$$

The effective energy parameter ϵ_{ij}^{LJ} ($i, j = 1, 2$, with 1 denoting CO_2 and 2 denoting the polymer monomer) is given by the relation $\int u_{ij}^{LJ}(\boldsymbol{r})d\boldsymbol{r} = \int u_{ij}^{PC}(\boldsymbol{r})d\boldsymbol{r}$, where u_{ij}^{PC} is the square well potential in PC-SAFT EOS.[5] σ_{ij} is the effective diameter of interaction. The cross interaction in PC-SAFT EOS is given by $\sigma_{ij} = (\sigma_i + \sigma_j)/2$, $\epsilon_{ij} = \sqrt{\epsilon_i\epsilon_j}(1 - k_{ij})$, $(i \neq j)$. In Table I, we list the value of molecular weight (M), chain length of polymer or average size of CO_2 cluster due to association interaction (N), energy parameter (ϵ), monomer diameter (σ), and k_{ij} parameter of PC-SAFT EOS for the species used in our model. These parameters are obtained by fitting the solubility value of EOS with the experimental data at different temperatures.[11,12] The temperature range for the validity of these parameters is also listed in Table I.

B. Perturbed-chain SAFT EOS

In PC-SAFT EOS,[5] the free energy density (f) of a fluid mixture is expressed as a summation of contributions from ideal gas (f_{id}), hard-sphere (f_{hs}), association (f_{assoc}), and dispersion effect (f_{disp}),

$$f = f_{id} + f_{hs} + f_{assoc} + f_{disp}. \quad (3)$$

The hard-sphere contribution is given by the EOS of Boublik[13] and Mansoori *et al.*,[14]

$$\beta f_{hs} = \frac{6}{\pi}\left[\frac{3\xi_1\xi_2}{1-\xi_3} + \frac{\xi_2^3}{\xi_3(1-\xi_3)^2} + \left(\frac{\xi_2^3}{\xi_3^2} - \xi_0\right)\ln(1-\xi_3)\right] \quad (4)$$

with $\xi_j = (\pi/6)\sum_{i=1,2}\rho_i\sigma_i^j$, $j = 0, 1, 2, 3$, where ρ_i is the number density of species i. The contribution of polymer chain connectivity and associating interaction of CO_2 is given by

$$\beta f_{assoc} = -\sum_{i=1,2}\frac{N_i - 1}{N_i}\rho_i \ln g_{ii}, \quad (5)$$

where $N_1 = 2$ is the average size of associating CO_2 clusters and N_2 is the polymer chain length, respectively. g_{ii} is the contact value of the correlation function between segments of specie i, given by

$$g_{ii} = \frac{1}{1-\xi_3} + \frac{3\xi_2\sigma_i}{2(1-\xi_3)^2} + \frac{\xi_2^2\sigma_i^2}{2(1-\xi_3)^3}.$$

The dispersion contribution is given by

$$\beta f_{disp} = -\pi\sum_{i,j=1,2}\rho_i\rho_j\left[2J_1\beta\epsilon_{ij}^{PC} + \bar{N}M^{-1}J_2(\beta\epsilon_{ij}^{PC})^2\right]\sigma_{ij}^3 \quad (6)$$

with

$$M = 1 + \bar{N}\frac{8\xi_3 - 2\xi_3^2}{(1-\xi_3)^2} + (1-\bar{N})\frac{20\xi_3 - 27\xi_3^2 + 12\xi_3^3 - 2\xi_3^4}{(1-\xi_3)^2(2-\xi_3)^2},$$

where $\xi_3 = (\pi/6)\sum_{i=1,2}\rho_i\sigma_i^3$ is the total packing fraction. J_1 and J_2 are the contribution from the integral of radial distribution function. Gross and Sadowski[5] expressed them as a six-order polynomials, given by

$$J_k = \sum_{i=0}^{6} a_i^{(k)}(\bar{N})\xi_3^i, \quad k = 1, 2$$

with the coefficients

$$a_i^{(k)} = a_{i0}^{(k)} + \frac{\bar{N}-1}{\bar{N}}a_{i1}^{(k)} + \frac{\bar{N}-1}{\bar{N}}\frac{\bar{N}-2}{\bar{N}}a_{i2}^{(k)},$$

where $\bar{N} = N_1 x + N_2(1-x)$ and x is the molar fraction of CO_2. These authors[5] obtained the constant coefficients $\{a_{ij}^{(k)} | k = 1, 2; i = 0, 1, \ldots, 6; j = 0, 1, 2\}$ by fitting the calculated binodal with experimental data for a great number of species.

In PC-SAFT EOS, there are three molecular model parameters (N, σ, and ϵ) that need to be determined for each species. In this work, the three parameters for CO_2 are obtained by fitting the PVT data of pure CO_2.[15] The parameters for PS and PMMA are then regressed by fitting the solubility data[11,12] of CO_2 in the mixtures at three different temperatures ($T = 373.2$ K, 413.2 K, and 453.2 K for PS; $T = 323.2$ K, 338.2K, and 353.2K for PMMA). The value

TABLE I. Parameters for the species studied in this work.

Species	M (g/mol)	N(–)	ϵ/k(K)	σ (Å)	$k_{ij}(\times 10^4)$[a]	Temperature range
CO_2	44	2	170.5	2.79	…	260-450 K
PMMA	89 230	2855	256.4	3.10	−339.36+1.05T	280-380 K
PS	160 000	4048	328.1	3.45	−227.65+0.61T	280-470 K

[a] k_{ij} is used to modify the cross interaction between the polymer and CO_2 in the mixture.

of the energy parameter is temperature dependent. We take it to be the average value at the three temperatures. The cross interactions between CO_2 and polymer are modified by $\epsilon_{ij} = \sqrt{\epsilon_i \epsilon_j}(1 - k_{ij}), (i \neq j)$ with assuming $k_{ij} = a + bT$, where a and b are constants. The values of a and b are determined by regressing the solubility data of CO_2 in the mixtures at all the three temperatures. The values of these parameters are listed in Table I. The ratio (M/N) between molecular weight and chain length are 31.25 for PMMA and 39.53 for PS, respectively. We comment that these values are the results of numerical regression, and do not necessarily correspond to the molecular weight of polymer unit. However, the value for PS is close to that obtained by Gross *et al.*[16] for mixtures of polymers and short alkanes.

C. Helmholtz free energy functional

In this section, we extend the Helmholtz free energy expression of EOS to the inhomogeneous case as a functional. Following the PC-SAFT EOS, the Helmholtz free energy functional F is expressed as a sum of an ideal term corresponding to an ideal gas of monomers and polymers free of non-bonded interactions, and an excess contribution accounting for the inter- and intramolecular interactions,

$$F = F^{\mathrm{id}}[\rho_1(\boldsymbol{r}), \hat{\rho}_2(\boldsymbol{r}^{N_2})] + F^{\mathrm{ex}}[\rho_1(\boldsymbol{r}), \hat{\rho}_2(\boldsymbol{r}^{N_2})], \tag{7}$$

where $\rho_1(\boldsymbol{r})$ is the density profile of CO_2. $\hat{\rho}_2(\boldsymbol{r}^{N_2})$is the multidimensional density profile of polymer chain, i.e., the joint density of all the N_2 segments of the polymer, which is related to the segmental densities ρ_{2i}, $(i = 1, 2, \ldots, N_2)$ by

$$\rho_2(\boldsymbol{r}) = \sum_{i=1}^{N_2} \rho_{2,i}(\boldsymbol{r}) = \sum_{i=1}^{N_2} \int \mathrm{d}\boldsymbol{r}^{N_2} \delta(\boldsymbol{r} - \boldsymbol{r}_i) \hat{\rho}_2(\boldsymbol{r}^{N_2}). \tag{8}$$

The ideal term of Helmholtz free energy is known exactly as

$$\begin{aligned} \beta F^{\mathrm{id}}[\rho_1(\boldsymbol{r}), \hat{\rho}_2(\boldsymbol{r}^{N_2})] = & \int \mathrm{d}\boldsymbol{r} \rho_1(\boldsymbol{r})[\ln \rho_1(\boldsymbol{r}) - 1] \\ & + \int \mathrm{d}\boldsymbol{r}^{N_2} \hat{\rho}_2(\boldsymbol{r}^{N_2})[\ln \hat{\rho}_2(\boldsymbol{r}^{N_2}) - 1] \\ & + \int \mathrm{d}\boldsymbol{r}^{N_2} \hat{\rho}_2(\boldsymbol{r}^{N_2}) \beta V_{\mathrm{B}}(\boldsymbol{r}^{N_2}). \end{aligned} \tag{9}$$

In PC-SAFT-based DFT, the excess Helmholtz free energy includes the contribution from excluded-volume effect, correlations due to association of intramolecular polymer chain connectivity and CO_2 molecules, and dispersion interactions,

$$F^{\mathrm{ex}} = F^{\mathrm{ex}}_{\mathrm{hs}} + F^{\mathrm{ex}}_{\mathrm{assoc}} + F^{\mathrm{ex}}_{\mathrm{disp\text{-}local}} + F^{\mathrm{ex}}_{\mathrm{disp\text{-}nonlocal}}. \tag{10}$$

The first three terms extend the corresponding bulk terms in Eq. (3) to spatially varying systems, whereas the last term is an additional contribution due to the long-range dispersion interaction that is only non-vanishing when the system is inhomogeneous. $F^{\mathrm{ex}}_{\mathrm{hs}}$ accounts for the excluded volume effect and is given by the fundamental measure theory[10,17]

$$\beta F^{\mathrm{ex}}_{\mathrm{hs}} = \int \mathrm{d}\boldsymbol{r} \phi_{\mathrm{hs}}[n_\alpha(\boldsymbol{r})] \tag{11}$$

with

$$\begin{aligned} \phi_{\mathrm{hs}}[n_\alpha(\boldsymbol{r})] = & -n_0 \ln(1 - n_3) + \frac{n_1 n_2 - \boldsymbol{n}_{\mathrm{V1}} \boldsymbol{n}_{\mathrm{V2}}}{1 - n_3} \\ & + \left[\frac{\ln(1 - n_3)}{12\pi n_3^2} + \frac{1}{12\pi n_3 (1 - n_3)^2} \right] \\ & \times (n_2^3/3 - n_2 \boldsymbol{n}_{\mathrm{V2}} \boldsymbol{n}_{\mathrm{V2}}), \end{aligned} \tag{12}$$

where $n_i[\{\rho_j(\boldsymbol{r}) | j = 1, 2\}], (i = 0, 1, 2, 3, \mathrm{V1}, \mathrm{V2})$ are the weight density functionals of Rosenfeld.[10] We note that for homogeneous system, FMT reduces to the Boublik-Mansoori EOS (Eq. (4)).[18] FMT usually provides an accurate description for inhomogeneous hard-sphere systems. However, it fails to describe the density profiles under strong confinement when at most one sphere can fit in the confinement direction.[19] Thus, FMT or any density functionals based on FMT are incapable of describing systems under such extreme confinement. Our work does not concern such systems. However, we note that Rosenfeld *et al.*[20] and Tarazona[19] have developed versions of functionals that can describe such strongly confined systems. In principle, our theory can be extended by replacing the hard-sphere term F_{hs} with these improved functionals to allow description of strongly confined systems, but doing so will require refitting the parameters listed in Table I for the revised EOS, which is beyond the scope of this work.

The weight density functional are also used to describe other short-range interactions such as association and the local part of the dispersion interactions. We adopt the weighted density approximation (WDA) to extend these terms to inhomogeneous states. The functionals $n_i[\{\rho_j(\boldsymbol{r}) | j = 1, 2\}]$ $(i = 0, 1, 2, 3)$ are the counterparts of the functions $\xi_i (i = 0, 1, 2, 3)$ in the bulk EOS for the spatially varying system. $\beta F^{\mathrm{ex}}_{\mathrm{assoc}}$due to correlation of polymer chain connectivity and associating interaction of CO_2 is given by[21]

$$\beta F^{\mathrm{ex}}_{\mathrm{assoc}} = \sum_{i=1}^{2} \frac{1 - N_i}{N_i} \int \mathrm{d}\boldsymbol{r} n_{0i} \ln g_{ii}, \tag{13}$$

where g_{ii} is the contact value of the correlation function between segments of specie i, given by

$$g_{ii} = \frac{1}{1 - n_3} + \frac{3}{2} \frac{n_2 \sigma_i}{(1 - n_3)^2} + \frac{1}{2} \frac{n_2^2 \sigma_i^2}{(1 - n_3)^3}.$$

The dispersion term is decomposed as the sum of a local contribution $F^{\mathrm{ex}}_{\mathrm{disp\text{-}local}}$and a nonlocal contribution $F^{\mathrm{ex}}_{\mathrm{disp\text{-}nonlocal}}$. The local contribution from EOS is given by

$$\begin{aligned} \beta F_{\mathrm{disp\text{-}local}} = & -\pi \sum_{i,j=1,2} \int \mathrm{d}\boldsymbol{r} n_{0i}(\boldsymbol{r}) n_{0j}(\boldsymbol{r}) \\ & \times \left[2 J_1(\boldsymbol{r}) \beta \epsilon_{ij}^{\mathrm{PC}} + \bar{N} M^{-1}(\boldsymbol{r}) J_2(\boldsymbol{r}) (\beta \epsilon_{ij}^{\mathrm{PC}})^2 \right] \sigma_{ij}^3 \end{aligned} \tag{14}$$

with

$$M(\boldsymbol{r}) = 1 + \bar{N}\frac{8n_3 - 2n_3^2}{(1-n_3)^2} + (1-\bar{N})\frac{20n_3 - 27n_3^2 + 12n_3^3 - 2n_3^4}{(1-n_3)^2(2-n_3)^2},$$

$$J_k(\boldsymbol{r}) = \sum_{i=0}^{6} a_i^{(k)}(\bar{N}) n_3^i, \quad k = 1, 2.$$

The WDA alone does not sufficiently describe the long-range intermolecular attractions.[22] The additional long-range dispersion contributions due to spatial inhomogeneity are included in a mean-field manner by[23]

$$F^{\text{ex}}_{\text{disp-nonlocal}}[\rho_1(\boldsymbol{r}), \rho_2(\boldsymbol{r})] = \frac{1}{4}\sum_{i,j=1,2}\iint \mathrm{d}\boldsymbol{r}\mathrm{d}\boldsymbol{r}' g_{ij}(|\boldsymbol{r}-\boldsymbol{r}'|)u_{ij}(|\boldsymbol{r}-\boldsymbol{r}'|) \times [\rho_i(\boldsymbol{r}) - \rho_i(\boldsymbol{r}')][\rho_j(\boldsymbol{r}) - \rho_j(\boldsymbol{r}')]. \quad (15)$$

This form ensures that $F^{\text{ex}}_{\text{disp-nonlocal}}$ vanishes for the uniform bulk state and hence does not over account the contribution included in the bulk EOS. The pair distribution function is approximated by a step-function $g_{ij}(\boldsymbol{r}) = \Theta(\boldsymbol{r} - \sigma_{ij})$, which corresponds to the limit of zero density in the reference fluid. Because of the long-range nature of the dispersion interaction, we expect that this approximation that essentially amounts to averaging out oscillations in the g_{ij} should be a reasonable one.

D. Euler-Lagrange equations

The grand potential W of the system is related to the Helmholtz free energy functional as

$$W = F - \mu_1\int \rho_1(\boldsymbol{r})\mathrm{d}\boldsymbol{r} - \mu_2\int \hat{\rho}_2(\boldsymbol{r}^{N_2})\mathrm{d}\boldsymbol{r}^{N_2}, \quad (16)$$

where μ_1 and μ_2 are the chemical potential of CO_2 and the polymer chain, respectively. At equilibrium, the grand potential is minimized,

$$\frac{\delta W}{\delta\rho_1(\boldsymbol{r})} = \frac{\delta W}{\delta\hat{\rho}_2(\boldsymbol{r}^{N_2})} = 0. \quad (17)$$

Combining Eqs. (7), (8), (16), and (17) yields the Euler-Lagrange equations

$$\rho_1(\boldsymbol{r}) = \frac{1}{N_1}\exp\left[\beta\mu_1 - \frac{\delta\beta F^{\text{ex}}}{\delta\rho_1(\boldsymbol{r})}\right], \quad (18)$$

$$\rho_2(\boldsymbol{r}) = \exp\left[\beta\mu_2 - \frac{\delta\beta F^{\text{ex}}}{\delta\rho_2(\boldsymbol{r})}\right]\sum_{i=1}^{N_2} I_i(\boldsymbol{r})I_{N_2+1-i}(\boldsymbol{r}), \quad (19)$$

where the recursive function is given by

$$I_i(\boldsymbol{r}) = \begin{cases} 1 & , i = 1 \\ \dfrac{1}{4\pi\sigma_2^2}\displaystyle\int_{|\boldsymbol{r}-\boldsymbol{r}'|=\sigma_2}\mathrm{d}\boldsymbol{r}'\exp\left[-\dfrac{\delta\beta F^{\text{ex}}}{\delta\rho_2(\boldsymbol{r}')}\right]I_{i-1}(\boldsymbol{r}'), & i > 1 \end{cases}. \quad (20)$$

Equations (18)–(20) provide the key equations for calculating the density profiles in an inhomogeneous CO_2-polymer mixture.

Because the propagator function $I_i(\boldsymbol{r})$ is defined in terms of individual polymer segments, the numerical iteration becomes computationally intensive for a long polymer chain. Solution of the recursive relation of Eq. (20) reveals that the end effect becomes insignificant as the segment index increases for sufficiently large i, that is, $I_i(\boldsymbol{r}) \approx I(\boldsymbol{r})$ becomes independent of the segment index. Therefore, for a long homopolymer chains, we make the approximation $I_i(\boldsymbol{r}) \approx I_{100}(\boldsymbol{r})$ for $i > 100$. The end effect at the other end of chain is described by the symmetric expression of Eq. (20). This simplification considerably accelerates the convergence of the iterations and enables us to investigate systems with very long polymer chains.

The details of the numerical procedure for solving Eqs. (18)–(20) are identical to those used in our earlier work on the PR-based DFT;[1] we refer interested readers to that reference.

III. RESULTS AND DISCUSSION

We first examine the bulk phase behavior to establish the range of applicability of the PC-SAFT EOS based DFT. Figure 1 shows the solubility data of CO_2 in polystyrene (PS) and poly (methyl methacrylate) (PMMA). For comparison, we also include the results from the Peng-Robinson-SAFT EOS.[2] Both PC-SAFT and PR-SAFT EOSs yield satisfactory results for CO_2 solubility in bulk PS and PMMA, with comparable level of agreement with experimental data. The agreement is slightly better for the PC-SAFT EOS. At high pressures ($P > 35$ MPa), however, the PR-SAFT EOS produces some unphysical features with regard to the relative locations of the coexistence curves and the spinodal curves1. In density-density phase diagram, the binodal curves terminate at an end point at high pressure. Above that pressure, the spinodal curves extend beyond the region enclosed by binodal curves. This unphysical behavior is due to the poor description of excluded volume effect by PR-EOS.[3] The unphysical feature disappears when the phase diagram is calculated using the PC-SAFT EOS. In Figure 2(a), we show the density-density phase diagram using PC-SAFT EOS for PMMA-CO_2 mixtures at $T = 363.15$ K. The spinodal curves now stay inside the region enclosed by the binodal curves. This result demonstrates that the PC-SAFT EOS better captures the local packing effects at high densities than the PR-SAFT EOS.

To further investigate the phase behavior, we examine the phase boundaries in the $P-T$ plane. Figure 2(b) shows the coexistence lines of pure components and the two critical lines for PMMA-CO_2 mixtures in $P-T$ plane. The results reveal that the phase behavior is of Type III in the classification of van Konynenburg and Scott.[3] The critical line I emerges from the critical point of pure CO_2 and terminates at an end point. There it connects to a triple line, on which, a PMMA-rich phase coexists with a CO_2-rich vapor and a CO_2-rich liquid phase. As the temperature decreases, the triple line merges with the coexistence curve of pure CO_2. The critical line II

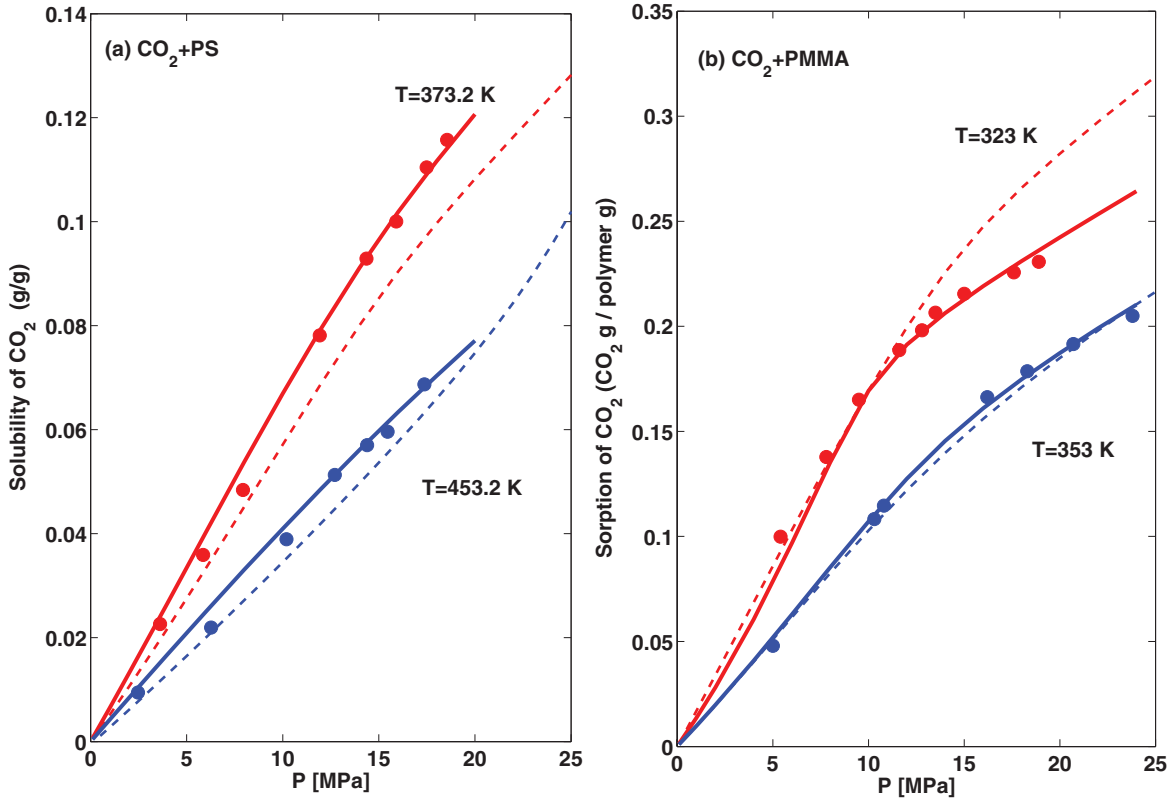

FIG. 1. Solubility of CO_2 in PS and PMMA. The solid lines are the results of PC-SAFT EOS and the dashed lines are the results of PR-SAFT EOS.[2] The solid circles are the experimental data.[11,12]

emerges from the critical point of the pure PMMA and moves up in pressure with decreasing temperature. In the region near the critical point of pure PMMA, the polymer-rich liquid coexists with the CO_2-rich vapor at the binodal of the mixture. As the temperature is decreased, the phase coexistence gradually changes its character to a coexistence of polymer-rich liquid and CO_2-rich liquid in the region near the pure CO_2 critical point. Due to the competition between these two types of

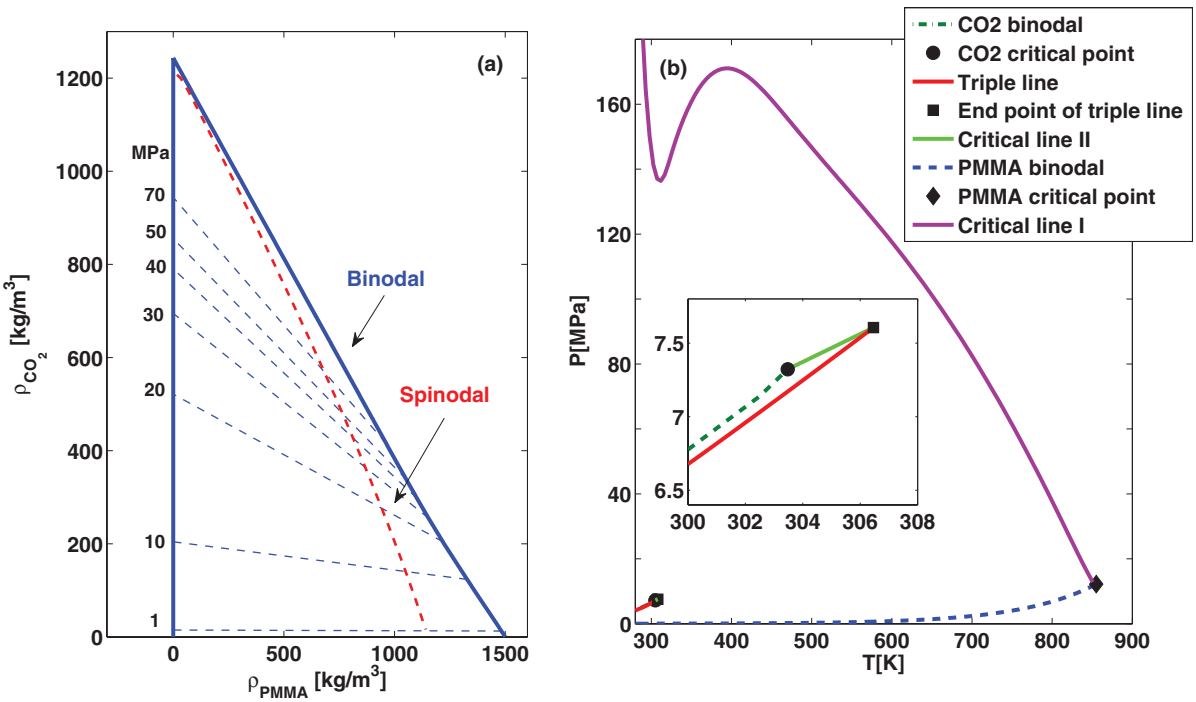

FIG. 2. (a) Density-density phase diagram of PMMA-CO_2 mixture at $T = 363.15$ K. The blue solid lines are the binodal curves and the red dashed lines are the spinodal curves. The blue dashed lines are the tie lines of phase coexistence. (b) Coexistence lines of the pure components (dashed lines) and critical and triple lines of PMMA-CO_2 mixtures (solid lines) in the $P-T$ plane.

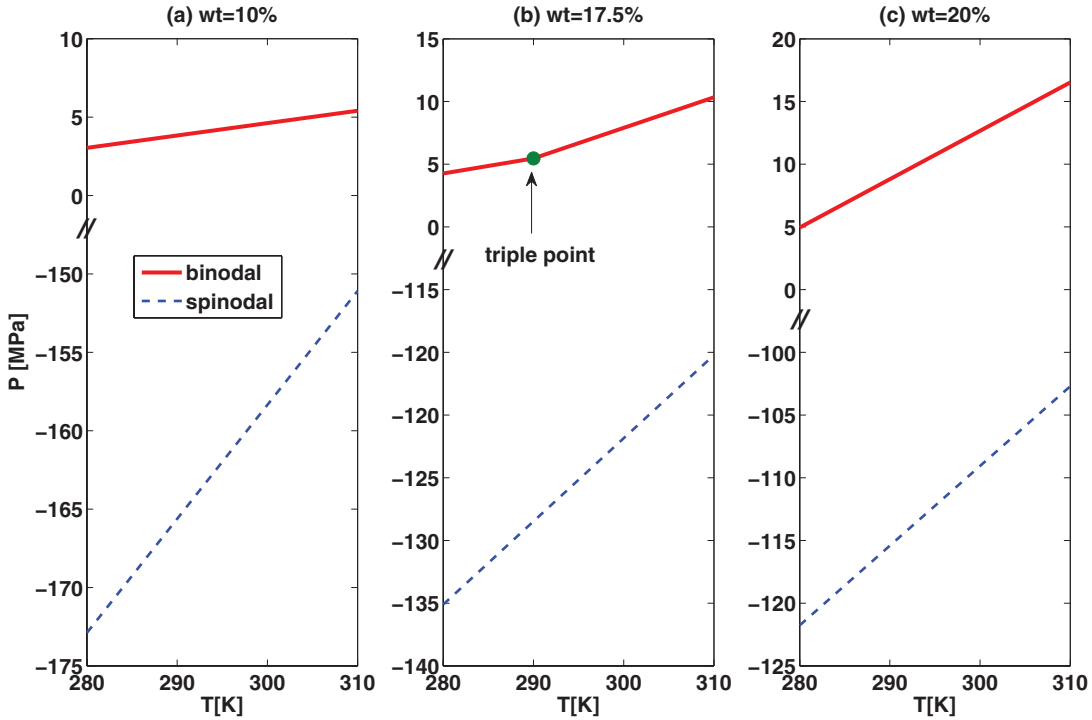

FIG. 3. $P-T$ phase diagram of PMMA-CO_2 mixtures at CO_2 weight fraction of (a) wt = 10%, (b) wt = 17.5%, and (c) wt = 20%.

phase coexistence, critical line II has a local minimum around the critical temperature of CO_2.

The liquid-vapor phase behavior of polymer and CO_2 mixtures depends strongly on the composition. The relative location of the spinodal and binodal curves is an important factor in the study of bubble nucleation. Figure 3 shows the $P-T$ phase diagram at several CO_2 weight fractions $wt = m_1/(m_1 + m_2)$, where m_1 and m_2 are the weight of CO_2 and polymer in liquid phase, respectively. At low weight fraction, the mixtures behave similarly to pure polymer. The binodal pressure increases slightly with the temperature and the spinodal curve is at very negative pressures and is far away from the binodal curve. (Note that the pressures scales are not the same on the three panels.) For higher weight fractions, the increase in the binodal pressure with temperature is more significant and the distance between binodal and spinodal is also reduced. At wt = 17.5 %, there appears a triple point at $T = 290$ K, at which, the polymer-rich phase coexists with CO_2-vapor and CO_2-liquid phase.

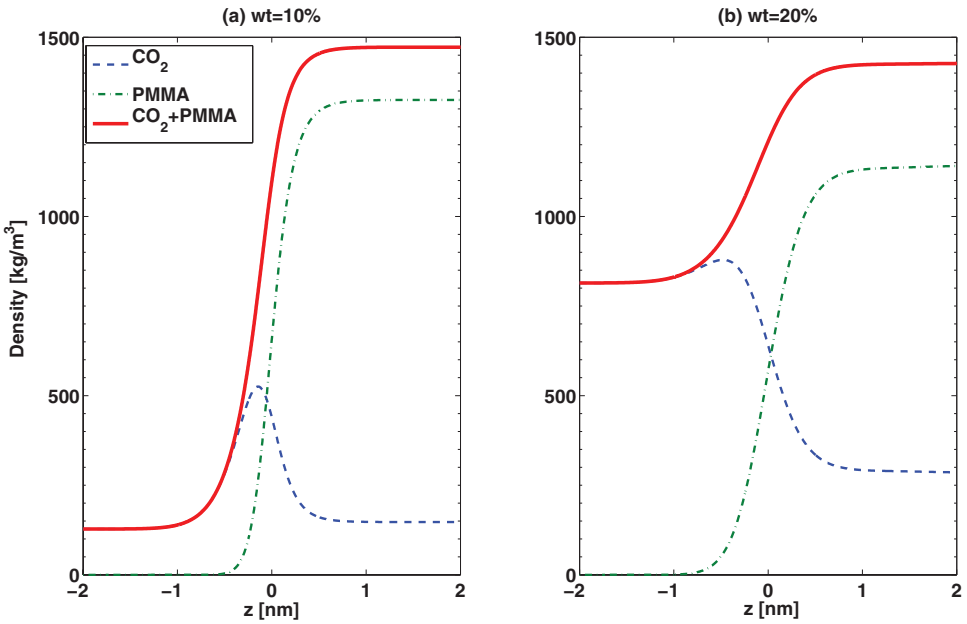

FIG. 4. Density profiles across the coexisting interface for PMMA-CO_2 mixtures at $T = 310$ K.

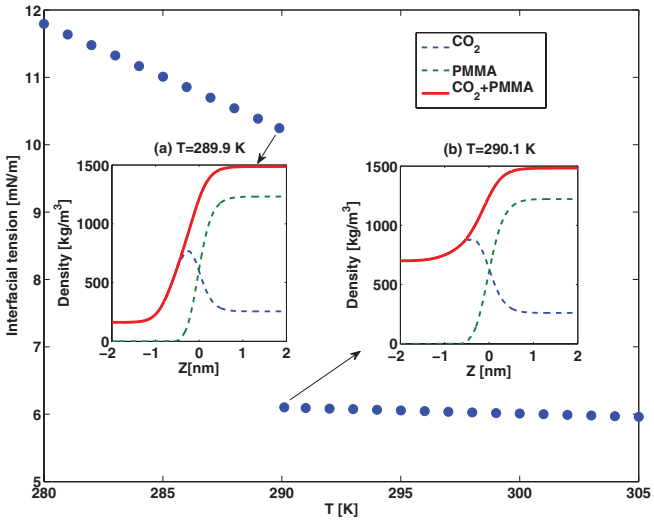

FIG. 5. Interfacial tension between the polymer rich phase and the CO_2-rich phase for PMMA-CO_2 mixtures at wt = 17.5%. The insets show the density profiles between coexisting phases near the triple point at (a) $T = 289.9$ K and (b) $T = 290.1$ K. The triple-point temperature is 290 K.

Having obtained a global view of the bulk phase behavior, we now apply our DFT to investigate the interfacial properties at the liquid-vapor coexistence. Figure 4 shows the density profiles between PMMA-rich liquid and the CO_2-rich vapor at $T = 310$ K; the weight fraction in the figures refer to that in the PMMA-rich liquid. For the lower weight fraction wt = 10%, there is a sharp change in the PMMA density across the interface. The density of CO_2 is nearly equal in the two phases, with a notable surface enhancement at the interface. For the higher weight fraction wt = 20%, the density of CO_2 in the CO_2-rich side (left side) is higher and is liquid. The PMMA density change is more gradual across the interface; the interfacial region is broader.

Interfacial tension is one of the most important physicochemical properties for polymer-CO_2 mixtures for many practical applications. The interfacial tension at a planar interface is calculated from $\gamma = (W - W_{\text{bulk}})/A$, where W_{bulk} is the grand potential in bulk phase and A is the surface area. Figure 5 shows the interfacial tension of the coexisting phase as a function of temperature at wt = 17.5 %. At this composition, increasing the temperature can take the system across the triple point; see Figure 3(b). The overall decrease of the interfacial tension with the temperature is expected as the interface becomes broader. At the triple point ($T = 290$ K), there is a discontinuity in the curve of interfacial tension. For $T < 290$ K, the PMMA-rich phase coexists with a CO_2-vapor, while $T > 290$ K it coexists with a CO_2 liquid phase. As temperature further increases above 290 K, the interfacial tension decreases slowly and eventually vanishes at the liquid-liquid critical point $T_c = 794.1$ K. (This value is not to be taken as accurate because it is well outside the limited range of temperatures in which the data regression is performed to determine the model parameters.) In the insets, we show the interfacial profiles across on the two sides of the triple point. At $T = 289.9$ K, the density of CO_2 corresponds to a vapor while at $T = 290.1$ K, the density of CO_2 in the CO_2-rich side becomes a liquid phase. In Figure 6, we compare the predicted values of the interfacial tension with experimental data for both PS-CO_2 and PMMA-CO_2 mixtures. The results of PR-SAFT-based DFT are also included for comparison. At these conditions, the CO_2-rich phases are in the vapor state. In general, both theories capture the experimental results quite well. The two versions of DFTs yield comparable agreement for the PS-CO_2 system, but the PC-SAFT-based DFT clearly gives better agreement for PMMA than the PR-SAFT-based DFT.

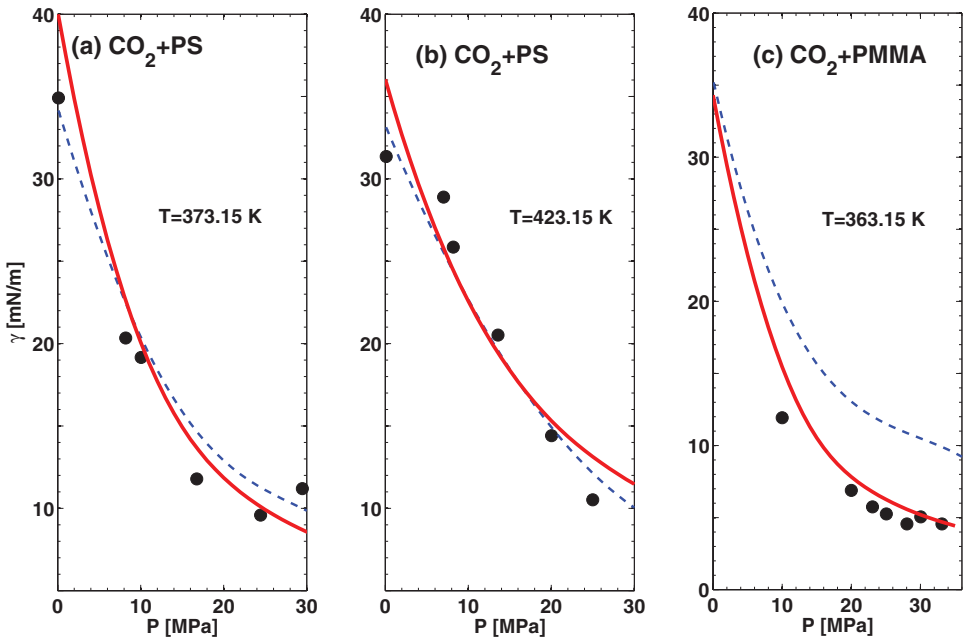

FIG. 6. Interfacial tension between polymer-rich phase and CO_2-rich phase as a function of pressure. The solid lines are the results of PC-SAFT-based DFT, and the dashed lines are the results of PR-SAFT-based DFT. The solid circles are the experimental data.[24,25]

IV. CONCLUSIONS

In this work, we have proposed a density-functional theory (DFT) based on the perturbed-chain statistical associating fluid theory equation of state (PC-SAFT EOS) for describing inhomogeneous polymer-carbon dioxide mixtures. The weight density functions from fundamental measure theory are used to extend the bulk excess Helmholtz free energy to the inhomogeneous case. The additional long-range dispersion contributions are included using a mean-field approach. The functional is fully consistent with the free energy in PC-SAFT EOS and reduces to it in the homogeneous bulk limit. The DFT is applied to the interfacial properties of polystyrene-CO_2 and poly(methyl methacrylate) CO_2 systems. The calculated values of the interfacial tension are in excellent agreement with experimental data. Both PR-SAFT-based DFT and PC-SAFT-based DFTs yield comparable agreement for the PS-CO_2 system, but the PC-SAFT-based DFT is clearly superior to the PR-SAFT-based DFT for PMMA. PC-SAFT EOS is widely used in engineering applications for describing liquids and liquid mixtures of chain molecules. This work extends the bulk PC-SAFT EOS to the description of inhomogeneous polymer-CO_2 mixtures without introducing any additional parameters. Our PC-SAFT EOS-based DFT allows a unified treatment of bulk phase behavior and interfacial properties, and judged from the excellent quantitative performance, represents the most accurate theory for describing the thermodynamics of polymer-CO_2 mixtures. Compared with a Peng-Robinson-SAFT EOS-based DFT we developed earlier, the current DFT is free of the unphysical features at high pressures (around 35 MPa or more) and can therefore be used to study such high-pressure phenomena as polymer foaming by pressurized CO_2.

ACKNOWLEDGMENTS

The Dow Chemical Company is acknowledged for funding and for permission to publish the results. The computing facility on which the calculations were performed is supported by an NSF-MRI grant, Award No. CHE-1040558.

[1]X. F. Xu, D. E. Cristancho, S. Costeux, and Z. G. Wang, "Density functional theory for polymer carbon dioxide mixtures," Ind. Eng. Chem. Res. **51**, 3832–3840 (2012).
[2]H. Y. Shin and J. Z. Wu, "Equation of state for the phase behavior of carbon dioxide polymer systems," Ind. Eng. Chem. Res. **49**, 7678–7684 (2010).
[3]P. H. van Konynenburg and R. L. Scott, "Critical lines and phase-equilibria in binary vanderwaals mixtures," Philos. Trans. R. Soc. London, Ser. A **298**, 495–540 (1980).
[4]M. Müller, L. G. MacDowell, P. Virnau, and K. Binder, "Interface properties and bubble nucleation in compressible mixtures containing polymers," J. Chem. Phys. **117**, 5480–5496 (2002).
[5]J. Gross and G. Sadowski, "Perturbed-chain SAFT: An equation of state based on a perturbation theory for chain molecules," Ind. Eng. Chem. Res. **40**, 1244–1260 (2001).
[6]N. F. Carhahan and K. E. Starling, "Equation of state for nonattracting rigid spheres," J. Chem. Phys. **51**, 635–636 (1969).
[7]G. Sadowski, "Modeling of polymer phase equilibria using equations of state," in *Polymer Thermodynamics Liquid Polymer-Containing Mixtures*, Advances in Polymer Science Vol. 238, edited by S. Enders, and B. Wolf (Springer-Verlag, Berlin, 2011), pp. 389–418.
[8]M. Kleiner, F. Turnakaka, and G. Sadowski, "Thermodynamic modeling of complex systems," in *Molecular Therodynamics of Complex Systems*, Structure and Bonding Vol. 131, edited by X. Lu, and Y. Hu (Springer-Verlag, Berlin, 2009), pp. 75–108.
[9]J. Gross, "A density functional theory for vapor-liquid interfaces using the PCP-SAFT equation of state," J. Chem. Phys. **131**, 204705 (2009).
[10]Y. Rosenfeld, "Free-energy model for the inhomogeneous hard-sphere fluid mixture and density-functional theory of freezing," Phys. Rev. Lett. **63**, 980–983 (1989).
[11]A. Rajendran, B. Bonavoglia, N. Forrer, G. Storti, M. Mazzotti, and M. Morbidelli, "Simultaneous measurement of swelling and sorption in a supercritical CO_2-poly(methyl methacrylate) system," Ind. Eng. Chem. Res. **44**, 2549–2560 (2005).
[12]Y. Sato, M. Yurugi, K. Fujiwara, S. Takishima, and H. Masuoka, "Solubilities of carbon dioxide and nitrogen in polystyrene under high temperature and pressure," Fluid Phase Equilib. **125**, 129–138 (1996).
[13]T. Boublik, "Hard-sphere equation of state," J. Chem. Phys. **53**, 471–472 (1970).
[14]G. A. Mansoori, N. F. Carhahan, K. E. Starling, and T. W. Leland, "Equilibrium thermodynamic properties of mixture of hard spheres," J. Chem. Phys. **54**, 1523–1524 (1971).
[15]R. Span and W. Wagner, "A new equation of state for carbon dioxide covering the fluid region from the triple-point temperature to 1100 K at pressures up to 800 mpa," J. Phys. Chem. Ref. Data **25**, 1509–1596 (1996).
[16]J. Gross and G. Sadowski, "Application of the perturbed-chain SAFT equation of state to associating systems," Ind. Eng. Chem. Res. **41**, 5510–5515 (2012).
[17]Y. X. Yu and J. Z. Wu, "Density functional theory for inhomogeneous mixtures of polymeric fluids," J. Chem. Phys. **117**, 2368–2376 (2002).
[18]R. Roth, "Fundamental measure theory for hard-sphere mixtures: a review," J. Phys. Condens. Matter **22**, 063102 (2010).
[19]P. Tarazona, "Density functional for hard sphere crystals: A fundamental measure approach," Phys. Rev. Lett. **84**, 694–697 (2000).
[20]Y. Rosenfeld, M. Schmidt, H. Lowen, and P. Tarazona, "Fundamental-measure free-energy density functional for hard spheres: Dimensional crossover and freezing," Phys. Rev. E **55**, 4245–4263 (1997).
[21]E. Klerlik and M. L. Rosinberg, "A perturbation density-functional theory for polyatomic fluids. 2. flexible molecules," J. Chem. Phys. **99**, 3950–3965 (1993).
[22]P. Tarazona, J. Cuesta, and Y. Martinez-Raton, "Density functional theory of hard particle systems," Lect. Notes Phys. **753**, 247 (2008).
[23]C. Ebner, W. F. Saam, and D. Stroud, "Density-functional theory of simple classical fluids. 1. surfaces," Phys. Rev. A **14**, 2264–2273 (1976).
[24]K. Otake, M. Kobayashi, Y. Ozaki, S. Yoda, Y. Takebayashi, T. Sugeta, N. Nakazawa, H. Sakai, and M. Abe, "Surface activity of myristic acid in the poly(methyl methacrylate)/supercritical carbon dioxide system," Langmuir **20**, 6182–6186 (2004).
[25]P. Jaeger, R. Eggers, and H. Baumgartl, "Interfacial properties of high viscous liquids in a supercritical carbon dioxide atmosphere," J. Supercrit. Fluids **24**, 203–217 (2002).